Bulgarian Chemical Communications, Volume 43, Number 3 (pp. 427 - 438) 2011

Mass transfer behaviour of a new liquid-liquid rotating screen disc extractor

A.S. Shehata, A.H. Elshazly*, A.A. Zaatout, G.H. Sedahmed

Chemical Engineering Department, Faculty of Engineering, Alexandria University, Alexandria, Egypt

Received May 5, 2010; revised January 3, 2011

The mass transfer behaviour of a rotating mesh disc contactor was studied by measuring the rate of mass transfer of acetic acid extraction from toluene solution by water. Variables studied were geometry parameters of the screen disc such as mesh number and wire diameter, rotation speed, physical properties of the solution, axial flow velocity and effect of the number of closely packed screens per disc. For a single rotating screen disc contactor the rate of mass transfer was expressed by the equation:

$$Sh_m = 132.63\, Sc^{0.33}\, \mathrm{Re}_S^{0.25}\, \mathrm{Re}_F^{0.3} \left(\frac{r_h}{d_w} \right)^{-1.38}$$

For rotating multi-screen discs, the mass transfer coefficient decreases by increasing the number of closely packed screens per disc. A comparison between the mass transfer behaviour of a rotating screen disc and a rotating solid disc contactor (RDC) revealed that for a given set of conditions the rate of mass transfer at the rotating screen contactor is higher than that of the rotating disc contactor by a factor of 13.8 – 28.4 depending on the operating conditions. Mechanical power consumption measurements showed that the higher the power consumption, the higher the mass transfer coefficient. Practical applications of the proposed extractor in fields such as pharmaceutical industry, hydrometallurgy, petroleum industry and water treatment were noted.

Key words: Mass transfer, rotating screen disc, solvent extraction, rotating fixed bed.

1. INTRODUCTION

Rotary agitated extraction columns such as the rotating disc contactor (RDC) are more efficient and possess better operational flexibility than conventional sieve plate, packed and spray columns; these advantages have led to the wide use of the RDC in the petroleum industry for furfural and sulfur dioxide extraction, propane deasphalting, solfolane extraction and caprolactum purification [1]. Since its invention by Reman [1, 2] in 1955, a lot of work has been done on various design and operational aspects of the RDC [1–12] such as

(i)-dispersed phase holdup along with drop size, which is necessary to calculate the interfacial area per unit volume; (ii)-slip velocity, which is required to estimate the mass transfer coefficient; (iii)-rate of mass transfer and axial dispersion coefficient required to correct the plug flow design. Modified versions of the RDC such as the asymmetric rotating disc extractor (ARD) [13–15], the open turbine rotating disc contactor (OTRDC) [16-19] and the rotating perforated disc contactor (RPDC) [20–26] have been developed. Wang *et al*. [21] demonstrated the superior performance of the modified rotating disc contactor over the traditional RDC. On the other hand, other authors [20] endeavored to expand the application of the RDC in extracting a variety of products such as cutinase [22], bovine serum albumin [23, 24] and trypsin [25]. Cavalcanti *et al*. [26] evaluated the performance of a perforated rotating disc contactor in extracting α-toxin from the fermented broth of *Clostridium perfringens* Type A by an aqueous two-phase system of polyethylene glycol–phosphate salts.

The aim of the present work was to explore the possibility of using rotating horizontal screen discs instead of rotating solid flat discs to make advantage of the high turbulence promoting ability of the screen in order to enhance the rate of mass transfer during extraction. To this end the rate of mass transfer of extraction of acetic acid from toluene (dispersed phase) by water (continuous phase) was chosen, as it has been widely used by different authors to evaluate the performance of extraction equipments. Previous studies on the use of screens to enhance the rate of mass transfer were limited to liquid-solid mass transfer [27–29].

2. EXPERIMENTAL SETUP AND PROCEDURE

2.1. Experimental setup

The apparatus (Figure 1) used in the present work consisted of a stainless steel cylindrical column agitated by rotating horizontal screen discs

*To whom all correspondence should be sent:
E-mail: Elshazly_a@yahoo.com

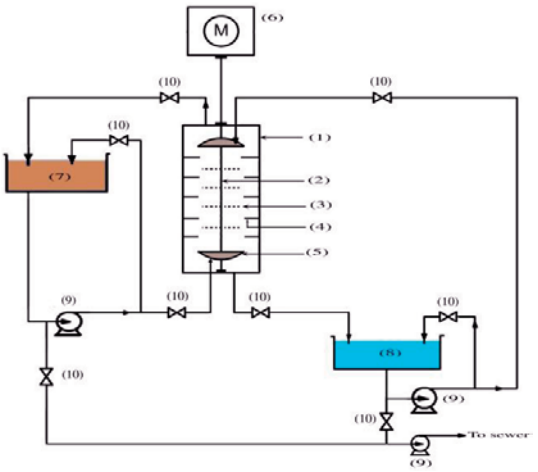

Fig. 1. Experimental setup. 1 - Agitated column; 2 - Rotating shaft; 3 - Rotating screen; 4 - Stator ring; 5 - Liquid distributor; 6 - Variable speed motor; 7 - Light phase storage tank; 8 - Heavy phase storage tank; 9 - Centrifugal pump; 10 - Control valve.

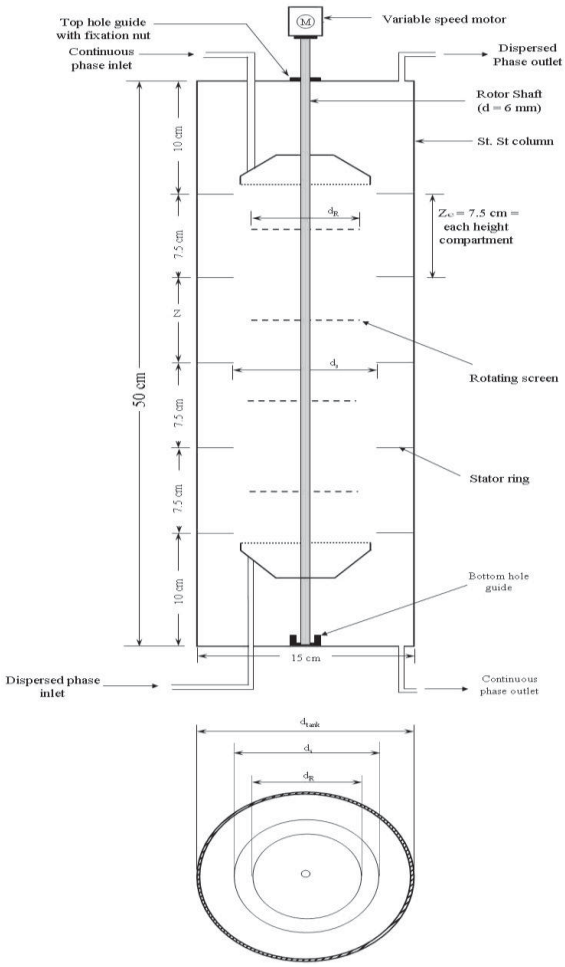

Fig. 2. Cross sectional view of the column

connected to a stainless steel shaft and driven by a digital D.C. (⅓ hp) motor, two glass storage tanks for both heavy phase (water) and light phase (toluene + acetic acid) and two stainless steel centrifugal pumps for driving liquids through the column. The stainless steel column has dimensions of 15 cm diameter, 50 cm height and 1 mm wall thickness. The column height was divided into four compartments formed by a series of stator rings connected to the column walls with rotating screens centered in each compartment. The dimensions of the column used in the present work conform to the standard dimensions [30] usually employed in designing extraction columns, column dimensions are related to column diameter (d_T) as follows:

Rotor screen diameter, d_R:

$$d_R = 0.5\ (d_T) \qquad (1)$$

Stator ring opening, d_S:

$$d_S = 0.67\ (d_T) \qquad (2)$$

Compartment height, Z_c:

$$Z_c = (0.12 - 0.5)\ (d_T) \qquad (3)$$

Column geometry factor G_f

$$G_f = \left[\left(\frac{Z_c}{d_R}\right)^{0.9}\left(\frac{d_s}{d_R}\right)^{2.1}\left(\frac{d_R}{d_T}\right)^{2.4}\right] \qquad (4)$$

In the present study, Z_c was equal to 0.5 d_T.

Based on the above equations and on the typical preferred ratios of various internal dimensions used by other authors [31], the dimensions of the column internals were selected for the rotating screen extractor column used in the present work as illustrated on Figure 2. The column was fitted with two flanged ends. The stator rings were held in position by welding to the inner column wall and they were placed longitudinally along the inner wall. The stator rings and the rotor screens were made of stainless steel sheet of 2 mm thickness. A stainless steel central shaft of 6 mm diameter holding the rotating screens was mounted through two holes to a guide connected to the lower and upper flanges, and it passes through a copper knob welded to the upper flange in order to support the shaft and prevent vibration during the operation. In addition, the nut was provided with a rubber gasket to prevent solution leakage during rotation of the shaft. The column end cover plates were provided with the necessary pipe connections for the inlet and outlet of the dispersed and continuous phase solutions. Each phase was introduced into the column through a distributor close to the first stator ring from the respective column ends. The exit pipes were flushed with the cover plates on the inside of the column as shown in Figure 2. Each flow circuit of both heavy and light phase consisted

of a 20 L glass storage tank and an ⅓ hp copper centrifugal pump which circulated the solution between the agitated column and the storage tank. The flow rates of both feed and solvent were adjusted by means of a bypass line and a plastic needle valve and were measured by collecting a definite volume of the solution in a definite time using a graduated cylinder and a stopwatch.

The system toluene – acetic acid – water was chosen for this work not only for the availability of materials, but for the availability of literature data on the system and the method of analysis. Toluene was nitration grade with a boiling range of 106 – 110ºC. Acetic acid was A.R. grade, and distilled water was used as a solvent and in preparing all solutions. 10 L of both feed (toluene – acetic acid solution) and solvent (water) were used in each run. The concentrations and the physical properties of the different feed solutions are given in Table 1 at 25ºC.

Table 1. Physical properties of the feed solutions used in the present study at 25°C

$C \times 10^3$ mole/cm^3	P g/cm^3	$\mu \times 10^2$ g/cm.s	$\upsilon \times 10^2$ cm^2/s	$D \times 10^5$ cm^2/s	$Sc = \frac{\upsilon}{D}$
0.1	0.861	0.56	0.6504	2.1	309
0.2	0.862	0.57	0.6613	2.06	320
0.3	0.863	0.58	0.6721	2.03	330
0.4	0.865	0.60	0.6936	1.96	354

2.2. Procedure

At the start of each run, the column was first filled with the heavy phase (water) and set at the desired flow rate, and then the speed of the rotor shaft was adjusted to the desired value, which ranged from 350 rpm to 1250 rpm. The light phase (toluene – acetic acid solution) was then introduced at the bottom end of the column and the flow rate was set at the desired value. Four different concentrations of acetic acid in toluene were used: 0.1, 0.2, 0.3 and 0.4 M. The rate of transfer of acetic acid from the organic to the aqueous phase was followed by withdrawing samples of 5 cm^3 from the aqueous phase (water) tank at 1 minute intervals for analysis by titrating against 0.1 N fresh sodium hydroxide solution using phenolphthalein as indicator. In all experiments, extraction took place from the toluene to the water and toluene was the dispersed phase.

All experiments were carried out at 25 ± 1ºC. Density and viscosity measurements of the solutions were performed using a density bottle and an Ostwald viscometer, respectively. Acetic acid diffusivity in toluene was obtained from the literature [32, 33] and was corrected for the change in viscosity using the Stokes – Einstein correlation:

$$\frac{D\mu}{T} = \text{constant} \quad [\text{g.cm.s}^{-2}.\text{K}^{-1}] \quad (5)$$

where: D is the diffusivity of acetic acid, (cm^2/s), μ is the solution viscosity, (g/cm.s) and T is the absolute temperature of the solution, (K)

Specifications of the screens used are shown in Table 2 where the screen specific area was calculated in terms of the wire diameter (d_w) and mesh number (N_m) using the method of Armour and Connon [34] as shown below.

Let (a) be the total screen surface area per total volume of one screen (cm^2/cm^3), then the value of (a) can be calculated from the equation:

Table 2. Specification of the screens used in the present study

Item	Screen geometry				
1	Mesh number (hole/in.)	10	14	18	22
2	Wire diameter, d_w (cm)	0.071	0.049	0.04	0.035
3	Screen thickness (cm)	0.142	0.098	0.08	0.07
4	Specific area (cm^2/cm^3)	12.842	17.936	23.14	28.433
5	Screen porosity, ε	0.772	0.78	0.768	0.751

$$a = \pi L N_m^2 \quad (6)$$

where:
$$L = \sqrt{\frac{1}{N_m^2} + d_w^2} \quad (7)$$

d_w = wire diameter, (cm)
N_m = mesh number (number of wires/cm)

The total screen area A_S is given by:

$$A_S = a\, n\, v_s \quad (8)$$

where: v_s is the volume of a single screen, n is the number of screens per array. In calculating the volume of the screen, the thickness is taken as twice the wire diameter ($2d_w$). In addition, the screen porosity can be calculated from the equation:

$$\varepsilon = 1 - \frac{\pi L N_m^2 d_w}{4} \quad (9)$$

In the present study five rotation speeds (350, 500, 750, 1000, 1250 r.p.m), screens of mesh number (10, 14, 18, 22 wire/in) were used; the number of closely packed screens per rotating disc was (1, 2, 3, 4, 5, screens/array), the initial concentrations of acetic acid in toluene were (0.1, 0.2, 0.3, 0.4 M) and five flow rates of the heavy phase (water) (79, 146, 174, 205, and 237 cm/s) were used. Mechanical power consumed in rotating the screens was measured experimentally under different conditions by means of a wattmeter. To compare between the performance of the present

rotating screen contactor (RSC) and the rotating disc contactor (RDC), experiments were carried out using a flat disc instead of a screen under different conditions.

3. RESULTS AND DISCUSSION

3.1. Mass Transfer at a Rotating Single Screen:

The volumetric mass transfer coefficient (*K*A) of the extraction of acetic acid from toluene with water in a batch rotating single screen contactor (Figure 1) was determined under different conditions: different screen rotation speed (r.p.m), different water flow rate (heavy continuous phase), different initial acetic acid concentration in toluene (light dispersed phase) and different mesh number of the rotating screen using the equation:

$$-\frac{dC}{dt} = \frac{KA}{V_s}\left(C_e - C\right) \qquad (10)$$

which upon integration yields:

$$\ln\frac{C_o - C_e}{C_e - C} = \left(\frac{KA}{V_s}\right)t \qquad (11)$$

where: C_o, C_e and C are the initial, equilibrium and current concentration of acetic acid in toluene, (mol/cm^3); K is the mass transfer coefficient, (cm/s); V_s is the volume of toluene, (cm^3) and A is the area of mass transfer, (cm^2). For simplicity, equation 11 can be written as:

$$\ln\frac{C_o - C_e}{C_e - C} = \left(\frac{K'}{V_s}\right)t \qquad (12)$$

where: $K' = KA$.

The volumetric mass transfer coefficient K' was calculated from the slope of the straight line obtained by plotting $\ln\frac{C_o - C_e}{C_e - C}$ *vs*. time as shown in Figure 3 under different operating conditions. Figures 4 and 5 show that the volumetric mass transfer coefficient increases with increasing the screen rotation speed according to the equation:

$$K' = aN^b \qquad (13),$$

where a and b are constants according to figures 4 and 5; the value of constant b ranges from 0.25 to 0.3.

The increase in the volumetric mass transfer coefficient with increasing screen rotational speed may be ascribed to the increase in the degree of turbulence generated by the rotating screen.

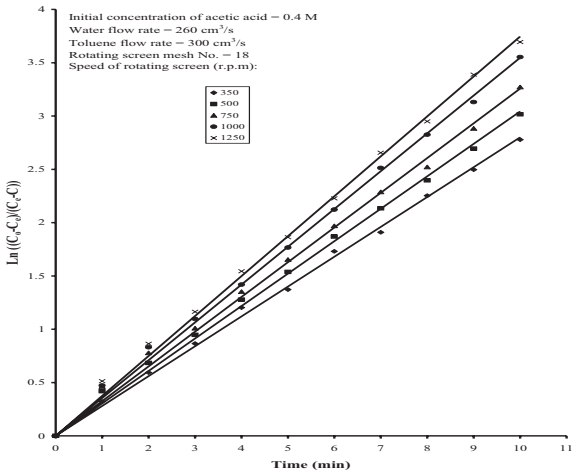

Fig. 3. ln $[(C_o-C_e)/(C-C_e)]$ *vs*. time for different speeds of the rotating screen.

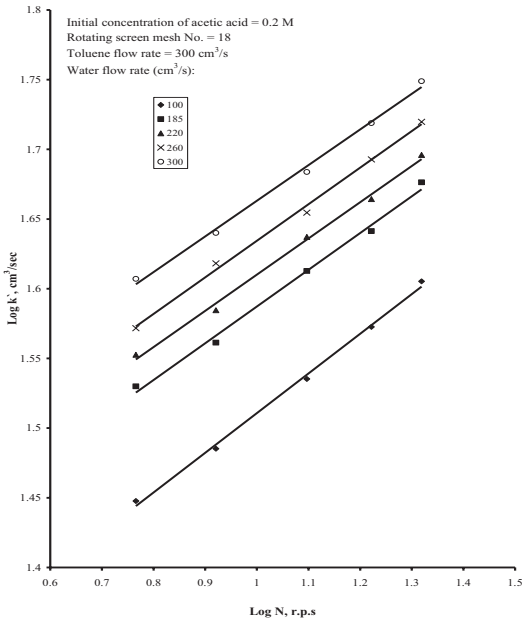

Fig. 4. log K\ *vs*. log N for different continuous phase flow rates.

Turbulence is generated when the wires of the rotating screen move through the solution because of boundary layer separation in the wake of the moving wires [35]. Turbulence is also generated when the flowing solution penetrates the screen [36, 37]. This turbulence enhances the rate of mass transfer between the organic phase and the aqueous phase via the following effects:

(i) Turbulence reduces the thickness (δ) of both organic phase and aqueous phase diffusion layers around the drop with a consequent increase in the mass transfer coefficient $K = D/\delta$.

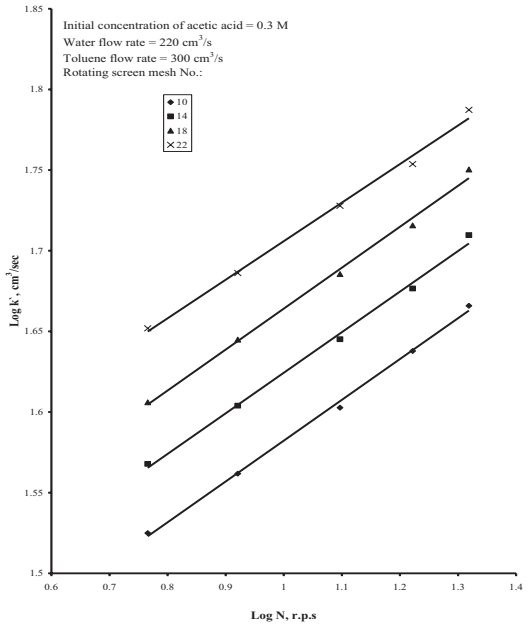

Fig. 5. log K\ *vs.* log N for different rotating screen mesh numbers.

(ii) The high shear stress arising from turbulence leads to rapid breakup and coalescence of the dispersed phase drops; the repeated coalescence and re-dispersion of drops enhances the rate of mass transfer through surface renewal [38].

(iii) The high shear stress also exercises drag at the interface between the drops and the continuous phase, this induces internal circulation inside the drops with a subsequent increase in the rate of mass transfer [39]. Whether internal circulation occurs depends on drop diameter and physical properties of the system, internal circulation does not take place when the drops become extremely small, extremely small drops behave as rigid spheres [39].

(iv) Turbulence increases the interfacial mass transfer area A by breaking large dispersed phase drops to the equilibrium size drops according to the equation:

$$A = \frac{6\psi}{d} \tag{14}$$

where ψ = dispersed phase holdup, and d = drop diameter.

The exponent (b) of equation 13 is less than the value (0.5) predicted from the penetration theory and the hydrodynamic boundary layer theory [38], the present exponent (0.25–0.33) is consistent with the value obtained for mass at stationary cylinders in cross flow at low Re where the velocity exponent ranges from 0.33 to 0.385 for 0.4< Re<40 (Re is based here on screen wire diameter). This similarity may underline the importance of the role played by the wake formed behind the screen wires as they rotate and are crossed by the axial flow [40]. The value of the exponent is also in a fair agreement with the value 0.358 obtained for the mass transfer at horizontal screens in cross flow [41]. Zaki *et al*. [42] who studied the mass transfer at horizontal vibrating screens found that the mass transfer coefficient increases with the 0.33 power of the vibration velocity. The authors explained this result based on similarity with mass transfer at cylinders in cross flow in the low Re range.

Figure 5 shows that the overall mass transfer coefficient increases by increasing the mesh number of the rotating screens. This may be explained as follows: (i) As the mesh number increases, the number of turbulence promoting wires increases with a consequent increase in the degree of turbulence which enhances the rate of mass transfer as mentioned before; (ii) as the screen opening decreases with increasing mesh number, jets of dispersed phase are formed through each opening as the solution flows across the screen, these jets interact and break down to give turbulence. Finally, this turbulence decays with distance away from the grid [36, 37]. The turbulence generated downstream the screen enhances the volumetric mass transfer coefficient via reducing the diffusion layer thickness and increasing the interfacial area (A) as mentioned before.

Figure 4 shows that the volumetric mass transfer coefficient increases by increasing the continuous phase (water) flow rate, which may be ascribed to the turbulence generated downstream of the rotating screen as the axial solution passes through the screen openings [36, 37]. The degree of turbulence generated downstream of the screen increases with increasing axial solution flow rate with a consequent increase in the mass transfer coefficient K and the interfacial area A as mentioned before.

Figure 6 shows that the rate of mass transfer increases by increasing initial solute (acetic acid) concentration; this can be attributed to the following: (i) As the mesh number increases, the number of turbulence promoting wires increases with a consequent increase in the degree of turbulence which enhances the rate of mass transfer as mentioned before; (ii) as the screen opening decreases with increasing mesh number, jets of dispersed phase are formed through each opening as the solution flows across the screen, these jets

interact and break down to give turbulence. Finally, this turbulence decays with distance away from the grid [36, 37]. The turbulence generated downstream the screen enhances the volumetric mass transfer coefficient via reducing the diffusion layer thickness and increasing the interfacial area (A) as mentioned before.

Figure 4 shows that the volumetric mass transfer coefficient increases by increasing the continuous phase (water) flow rate, which may be ascribed to the turbulence generated downstream of the rotating screen as the axial solution passes through the screen openings [36, 37]. The degree of turbulence generated downstream of the screen increases with increasing axial solution flow rate with a consequent increase in the mass transfer coefficient K and the interfacial area A as mentioned before.

Figure 6 shows that the rate of mass transfer increases by increasing initial solute (acetic acid) concentration; this can be attributed to the following:

As a result of the varying microscopic hydrodynamic conditions around dispersed phase drop, the rate of mass transfer of acetic acid from the drop surface is not uniform all over the drop surface. This leads to non-uniform concentration of acetic acid at the drop surface. Accordingly, the interfacial tension, which depends on solute concentration, will not be uniform all over the drop surface; surface tension will be high at locations with low acid concentration and low at locations with high acid concentration. This surface tension gradient gives rise to strong eruptions and interfacial turbulence at the drop surface (Marangoni effect) which enhances the rate of mass transfer [39]. Zhang *et al.* [32] who studied the extraction of acetic acid from water by toluene in a simple cell found that the enhancing effect of a surface tension driven flow increases with increasing acetic acid concentration, which is consistent with the present results.

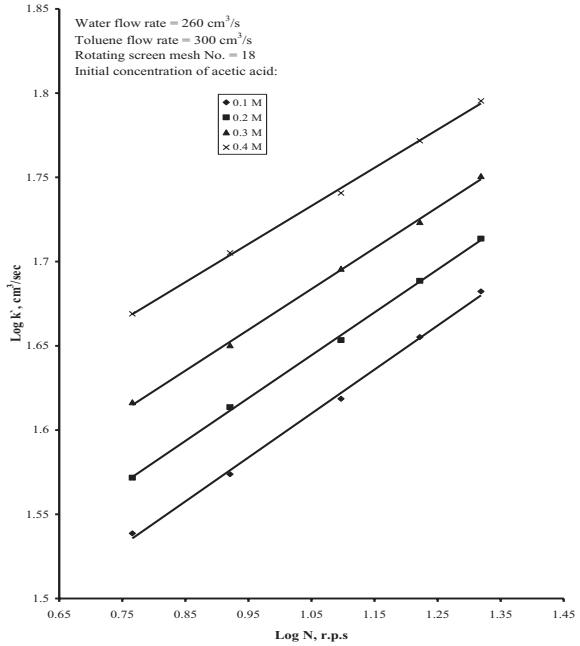

Fig.6. Log K` *vs*. log N for different initial concentrations of acetic acid.

3.2. Data Correlation

For the present case, dimensional analysis leads to the correlation:

$$Sh = a\, Sc^{\alpha}\, Re_S^{\beta}\, Re_F^{\gamma} \qquad (15)$$

The volumetric mass transfer coefficient will be used instead of the mass transfer coefficient, so a modified Sherwood number Sh_m will be used in the form:

$$Sh_m = \frac{K'}{d_R D} \qquad (16)$$

Rewriting Eq. (15) in the form:

$$Sh_m = a\, Sc^{\alpha}\, Re_S^{\beta}\, Re_F^{\gamma}\,, \qquad (17)$$

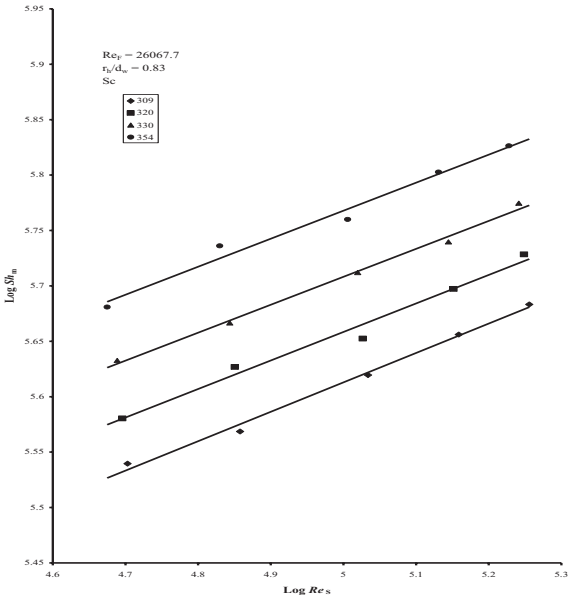

Fig. 7. log Sh_m *vs*. log Re_s for different Sc numbers.

following previous theoretical and experimental studies in mass transfer, the exponent α was fixed at 0.33 [40]. Figures 7 and 8 show the effect of Re_S on Sh_m at different Sc and different mesh number respectively. The data fit the equation:

$$Sh_m = a_1\, Re_S^{0.25} \qquad (18)$$

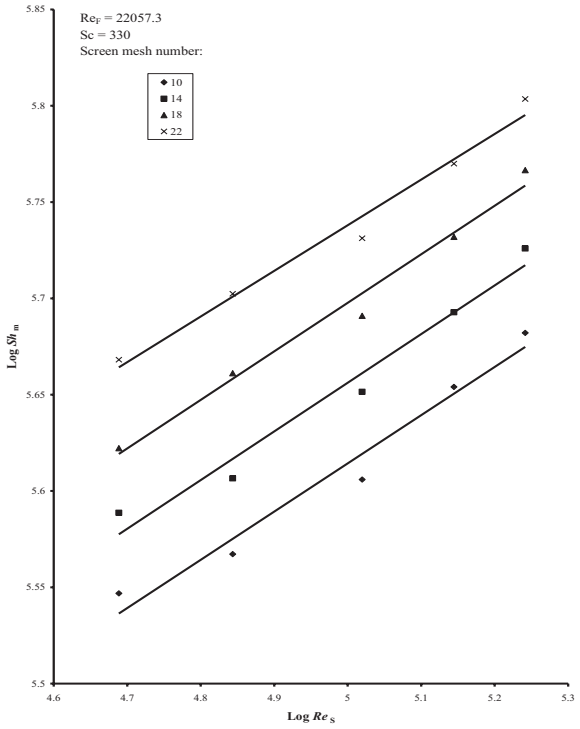

Fig. 8. log Sh_m *vs*. log Re_s for different screen mesh numbers.

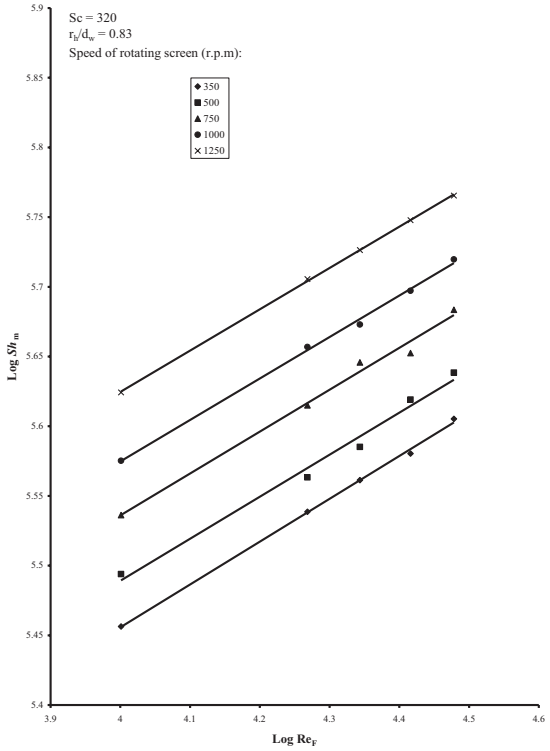

Fig. 9. log Sh_m *vs*. log Re_F for different speeds of rotating screen.

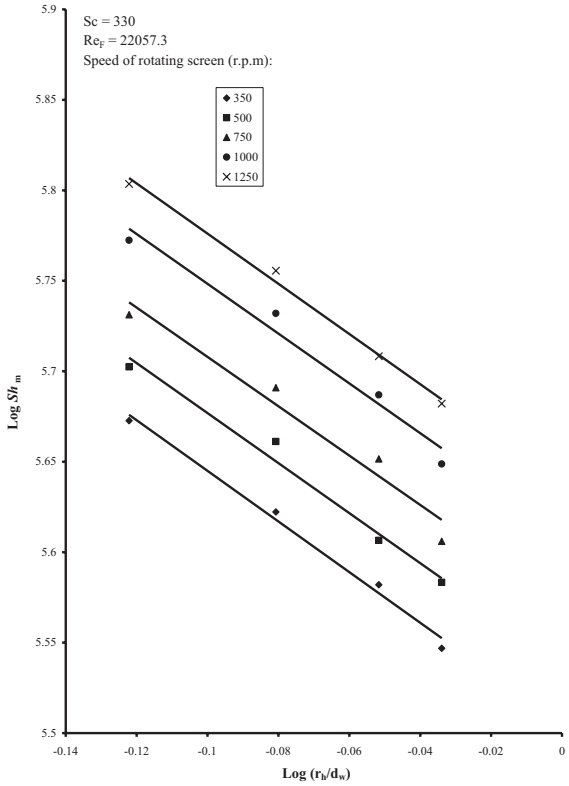

Fig. 10. log Sh_m *vs*. log (r_h/d_w) for different speeds of rotating screen.

Figure 9 shows the effect of Re_F on Sh_m at different rotation speeds, the data fit the equation:

$$Sh_m = a_2 \, Re_F^{0.30} \tag{19}$$

For the screens used in the present work, an extra dimensionless term which accounts for screen geometry should be added to eq. 17.

Screen geometry was expressed in terms of (r_h/d_w) [43] where r_h is the hydraulic radius defined as:

$$r_h = \frac{\varepsilon}{a} \tag{20}$$

where: ε is the screen porosity, a is the specific screen area (cm^2/cm^3) and d_w is the screen wire diameter. Figure 10 shows the effect of screen geometry (r_h/d_w) on Sh_m at different rotation speeds, the data fit the equation:

$$Sh_m = a_3 \left(\frac{r_h}{d_w} \right)^{-1.38} \tag{21}$$

Accordingly, equation 17 becomes:

$$Sh_m = a \; Sc^{0.33} \, Re_S^{0.25} \, Re_F^{0.30} \left(\frac{r_h}{d_w} \right)^{-1.38} \tag{22}$$

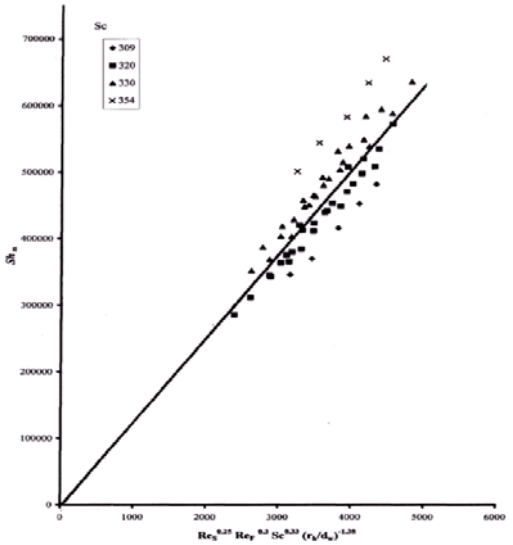

Fig. 11. Overall mass transfer correlation for the extraction of acetic acid from toluene by water using a rotating single screen contactor at different Sc numbers.

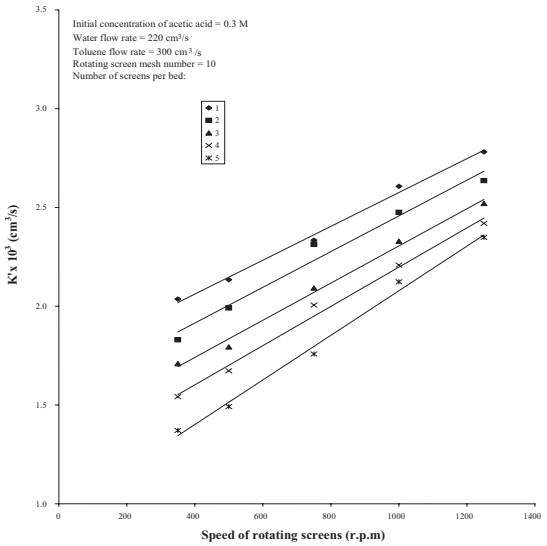

Fig. 12: Volumetric mass transfer coefficient *vs.* speed of rotating screen for different screen numbers per bed.

Figure 11 shows that the mass transfer data for the transfer of the solute from the dispersed phase to the continuous phase in a rotating single screen extractor under the conditions: 309 < *Sc* < 354, 47304 < Re_S < 180176, 10026 < Re_F < 30078 and 0.75 < r_h/d_w < 0.92, fit the equation:

$$Sh_m = 132.63\ Sc^{0.33}\ \mathrm{Re}_S^{0.25}\ \mathrm{Re}_F^{0.3}\left(\frac{r_h}{d_w}\right)^{-1.38} \qquad (23)$$

with an average deviation of ± 14%. The above equation can be used in the design and operation of a rotating screen liquid-liquid extractor.

3.3 Mass Transfer Rate at an Array of Closely Packed Screen

Figures 12 and 13 show the mass transfer behaviour of a rotating bed of closely packed horizontal screens under different conditions. The number of screens per bed ranged from 1 to 5. The results show that the mass transfer coefficient decreases below the value for a single screen with increasing number of screens per bed. These results agree with the finding of Sedahmed *et al.* [27] who studied liquid-solid mass transfer at a rotating fixed bed composed of closely packed screen discs. The mass transfer coefficient decreased below the single screen value increases slightly with increasing the mesh number. The percentage decrease in the rate of mass transfer ranges from 15.6 to 40.6% mainly depending on the bed thickness and the mesh number of the screen. The higher the mesh number of the screen the higher is the percent reduction in

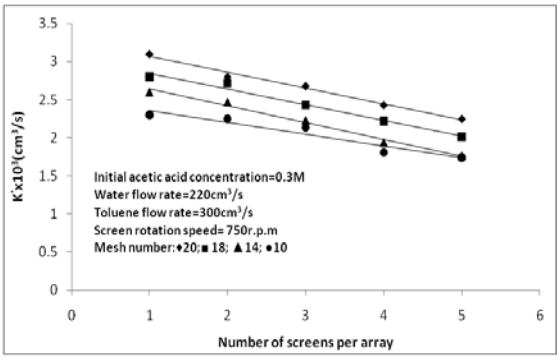

Fig. 13. Volumetric mass transfer coefficient *vs.* number of screens per array for different screen mesh numbers.

the mass transfer coefficient. The decrease in the mass transfer coefficient may be attributed to eddy damping by virtue of the friction between the generated eddies and the wires of the screen matrix.

3.4 Power Consumption

In order to assist in the economic evaluation of the performance of the present work, mechanical power consumed in rotating the screens was measured experimentally under different conditions by means of a wattmeter.

Mechanical power was measured for rotating closely packed arrays with a number of screens ranging from 1 to 5 at different rotational speeds. Figures 14 and 15 show the following results:

1. Power consumption increases with increasing screen rotation speed for all mesh numbers.
2. Power consumption tends to increase with increasing screen mesh number.

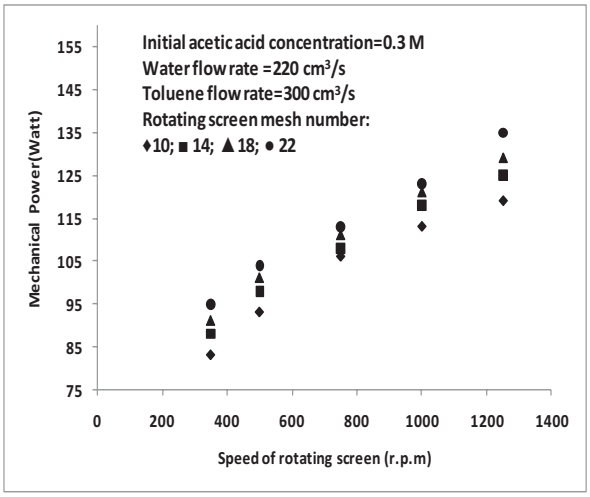

Fig. 14. Mechanical power consumption *vs.* speed of rotating screen for different rotating screen mesh numbers.

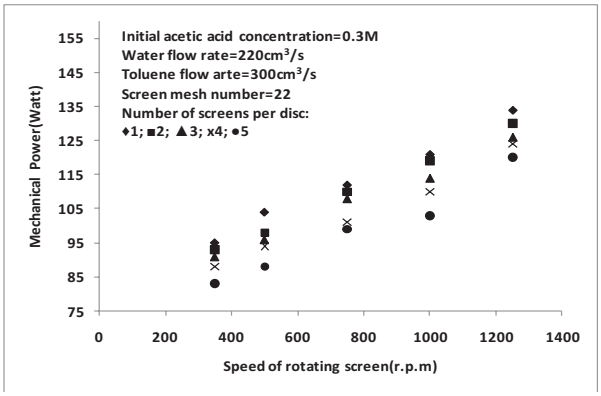

Fig. 15. Mechanical power consumption vs. speed of rotating screen for different screen numbers per bed.

3. Power consumption decreases with increasing the number of screens per array.

The results of power consumption and mass transfer coefficient at a rotating screen are in general consistent with the finding of Calderbank and MooYoung [44] who found that the mass transfer coefficient is proportional to power consumption, i.e., the higher the power consumption the higher the mass transfer coefficient. Figure 16 shows that the rotating screen of mesh number 10 is superior to screens with other mesh numbers because it produces higher mass transfer per unit power consumption.

3.5 Comparison between Rotating Screen Contactor (RSC) and Rotating Disc Contactor (RDC)

It would be of interest to compare the present mass transfer data for rotating screens with that for rotating flat discs. Figure 17 shows that the mass

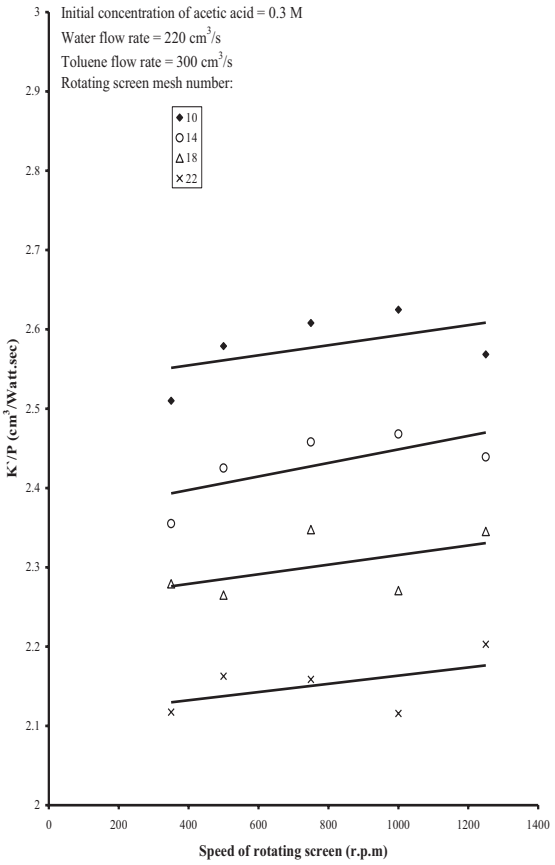

Fig. 16. The ratio ($K^{\backprime}$/P) *vs*. speed of rotating screen for rotating screens of different mesh numbers.

transfer coefficients for rotating screens are higher than those for rotating flat discs by an amount ranging from 1379 to 2839% depending on the rotation speed and mesh number of the screen. The above observations can be explained as follows: Both rotating solid discs and screen discs induce an axial flow towards the rotating surface [27, 31]. When the axial flow reaches the solid disc surface it turns to radial flow, but in case of rotating screens part of the axial flow induced by screen rotation turns to radial flow while the other part penetrates the screen in axial direction along with the superimposed net flow. Under such conditions, turbulence can be generated behind the screen wires because of boundary layer separation when the upward moving stream crosses the screen. The presence of eddies downstream of stationary screens in cross flow was revealed by Bourne and Lips [36] who studied the flow behaviour past stationary screens. In addition, turbulence could be also generated when the wires of the rotating screen move through the solution because of boundary layer separation in the wakes of the moving wires. Eddy generation increases the mass transfer coeffi-

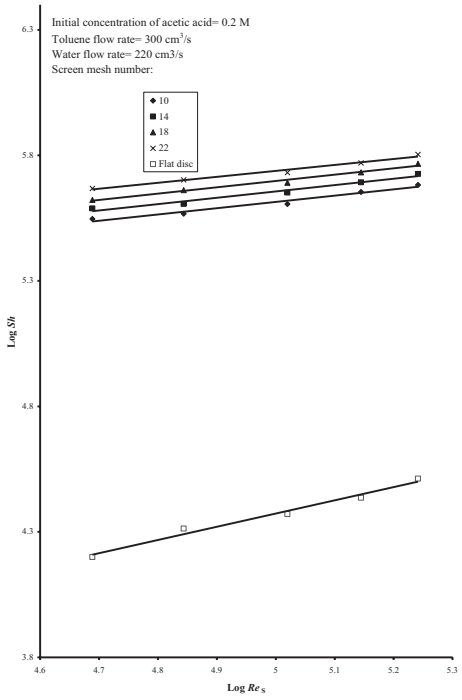

Fig. 17. log Sh *vs*. log Re_S for a rotating flat disc contactor and a rotating screen contactor with different mesh numbers.

cient at rotating screens compared to rotating discs where the radial flow at the disc surface is laminar within the present range of Re_S ($47304 < Re_S < 180176$)[45].

The superior mass transfer behaviour of a rotating screen contactor compared to the rotating disc contactor shows that the role played by the turbulence generated in the rotating screen contactor outweighs the high degree of axial mixing which characterizes the highly porous screen structure and which tends to reduce the rate of mass transfer.

4. CONCLUSIONS

The present study revealed that the performance of a screen disc extractor is superior to that of an ordinary rotating disc extractor owing to the turbulence promoting ability of rotating screens. The dimensionless mass transfer equation obtained in the present study can be used in the rational design and operation of the suggested rotating screen extractor. Further studies on different solvent extraction systems are needed to confirm the advantages of the present extractor compared to the rotating disc extractor and to validate its mass transfer behaviour under a wider range of operating conditions.

Nomenclature

A	Mass transfer area (cm^2)
A_S	Total screen area (cm^2)
a	Total screen surface area per total volume of one screen (cm^2/cm^3)
C, C_e, C_o	Current concentration, equilibrium concentration and initial acetic acid concentration in toluene (mol/cm^3)
D	Diffusivity (cm^2/s)
d	Drop diameter (cm)
d_R	Rotor screen diameter (cm)
d_S	Stator ring opening (cm)
d_T	Column diameter (cm)
d_w	Wire diameter (cm)
G_f	Column geometry factor
K	Mass transfer coefficient (cm/s)
$K^{\backslash}$	Volumetric mass transfer coefficient (cm^3/s)
N	Screen rotation speed (r.p.m)
N_m	Mesh number (number of wires/cm)
n	Number of screens per array
T	Absolute temperature of the solution (K)
V	Continuous phase velocity (cm/s)
V_s	Volume of toluene (cm^3)
Z_c	Compartment height (cm)

Dimensionless terms

Re_F	Reynolds number of continuous phase flow ($\rho_c V d_T/ \mu_c$)
Re_S	Reynolds number of the rotating screen disc ($\rho_d \omega d_R^2/ \mu_d$)
Sc	Schmidt number of dispersed phase ($\mu_d / \rho_d D$)
Sh	Sherwood number ($K d_R/D$)
Sh_m	Modified Sherwood number ($K^{\backslash}/d_R D$)
v_s	Volume of single screen (cm^3)

Greek symbols

α, β, γ	Constants
δ	Diffusion layer thickness (cm)
ε	Screen porosity
μ	Viscosity of the solution (g.cm/s)
μ_c	Viscosity of continuous phase (g.cm/s)
μ_d	Viscosity of dispersed phase (g.cm/s)
υ	Kinematic viscosity (cm^2/s)
ρ	Solution density (g/cm^3)
ρ_d	Density of dispersed phase (g/cm^3)
ρ_c	Density of continuous phase (g/cm^3)
ψ	Dispersed phase hold-up
ω	Screen rotational speed (rps)

REFERENCES

1. G.S. Laddha, T.E. Degaleesan, Transport Phenomena in Liquid-Liquid Extraction, McGraw Hill, New York, 1976.
2. W. C. G. Kosters, Rotating-disk Contactor, Handbook of Solvent Extraction Wiley, New York, UK, 1983.
3. W. J. Korchinsky, Rotating Disc Contactor Liquid-Liquid Extraction Equipment, John Wiley and Sons, Chichester, UK, 247, 1994.
4. R. W. Cusack, P. Fremeaux, *Chem. Eng. J.,* 132 (1991).
5. T. Misek, V. Rod, Calculation of Contactors with Longitudinal Mixing, Recent Advance in Solvent Extraction, Pergamon, New York, USA, 197, 1971.
6. M. Amanabadi, H. Bahmanyar, Z. Zarkeshan, M. A. Mousavian, *Chin. J. Chem. Eng.,* **17** (3), 366 (2009).
7. J. C. Godfrey, D. Houlton, K. R. M. Ramlochan, M. J. Slater, *Eng. Res. Des*., **79** (A2), 156 (2001).
8. A. Kumar, S. Hartland, *Can. J. Chem. Eng*., **70,** 77 (1992).
9. J. Venkataramana, T.E. Degaleesan G.S. Laddha, *Can. J. Chem. Eng.,* **58,** 206 (1980).
10. V.L. Pebalk, N.A. Gromov, M.I. D'yakova, A.E. Kostanyan, *J. Appl. Chem. USSR,* **59,** 1830 (1986).
11. L. Lu, Z. An, Z. Fan, J. Chen, J. *Chem. Ind. Eng. (CHINA)* (English Edition), **1** (2), 44 (1986).
12. S. H. Zhang, X. D. Ni, Y.F. Su, *Can. J. Chem. Eng.,* **59,** 573 (1981).
13. B.D. Kadam, J.B. Joshi, R.N. Patil, *Chem. Eng. Res. Des*., **87**, 756 (2009).
14. T. Misek, J. Marek, Handbook of Solvent Extraction, Wiley, New York, USA, 1983.
15. T. Misek, *Collect Czech Chem. Commun,* **40**, 1686 (1975).
16. J. W. Zhu, S.H. Zhang, X. K. Zhou, X. X. Chen, Y. F. Su, A. Vogelpohl, *Chem. Eng. Technol.,* **14**, 167 (1991).
17. X. X. Chen, H. T. Wang, K. H. Li, Y. F. Su, *J. Chem. Ind. Eng. (CHINA),* (English Edition), **7**, 28 (1992).
18. X. X. Chen, K. H. Li, Y.F. Su, *Ind. Eng. Chem. Res.* **32,** 453 (1993).
19. X. X. Chen, H. T. Wang, K. H. Li, Y. F. Su, *J. Chem. Ind. Eng. (CHINA),* **44**, 171 (1993).
20. S. Soltanali, Y. Z. Shirkolaee, G. H. Amoabediny, H. Rashedi, A. Sheikhi, P. Chamanrokh, *Chem. Eng. Sci*, **64** (10), 2301 (2009).
21. Y. D. Wang, W. Y. Fei, J. H. Sun, Y. K. Wan, *Chem. Eng. Res. Des.,* **80** (4), 392 (2002).
22. M. T. Cunha, M. J. L. Costa, C. R. C. Calado, L. P. Fonseca, M. R. Aires-Barros J. M. S. Cabral, *J. Biotechnol*., **100,** 55 (2003).
23. E. B. Tambourgi, J.A.F.R. Pereira, *Latin Am. Appl. Res*., **23,** 257 (1993).
24. A. L. F. Porto, L. A. Sarubbo, J. L. Lima-Filho, M. R. Aires-Barros, J. M. S. Cabral, E. B. Tambourgi, *Bioprocess Eng.*. **22,** 215 (2000).
25. L. A. Sarubbo, L. A. Oliveira, A. L. F. Porto, J. L. Lima-Filho, G. M. Campos-Takaki, E.B. Tambourgi, *Biochem. Eng. J.,* **16,** 221 (2003).
26. M. T. H. Cavalcanti, M. G. Carneiro-da-Cunha, I. V. Brandi, T. S. Porto, A. Converti , J. L. Lima Filho, A. L. F. Porto, A. Pessoa, *Chem. Eng. Process.,* **47**, 1771 (2008).
27. G. H. Sedahmed, M. Z. Al-Abd, Y. A. El-Taweel, M. A. Darwish, *Chem. Eng. J.,* **76** (3), 247 (2000).
28. M. M. Zaki, I. Nirdosh, G. H. Sedahmed, *Chem. Eng. J.,* **126** (2-3), 67 (2007).
29. A. H. Abbar, A. H. Sulaymon, M. G. Jalhoom, *Electrochim. Acta,* **53** (4), 1671 (2007).
30. A. S. Philip, Handbook of Separation Techniques for Chemical Engineers, 3rd ed., McGraw Hill, Inc., N.Y., 419, 1997.
31. G. S. Laddha, T. E. Degaleesan, R. Kannappan, *Can. J. Chem. Eng*., **56** (20), 137 (1978).
32. S. H. Zhnag, Z. M. Wang, Y. F. Su, *Trans IChemE*, **68** (84), 84 (1990).
33. C. R. Wilke, P. Chang, *AIChEJ,* **1**, 264 (1955).
34. J. C. Armour, J. N. Connon, *AIChE J,* **14** (3), 415 (1968).
35. J. G. Knudsen, D. L. Katz, Fluid Dynamics and Heat Transfer, McGraw Hill, N.Y., 1989.
36. J. R. Bourne, M. Lips, *Chem. Eng. J.,* **47** (3), 155 (1991).
37. E. Villermaux, J. Sommeria, Y. Gagne, E. J. Hopfinger, *Eur. J. Mech. B: Fluids*, **10** (4), 427 (1991).
38. D. Glasser, D. R. Arnold, A. W. Bryson and A. M. S. Vieler, *Miner. Sci. Eng*., **8** (1), 23 (1976).
39. T. K. Sherwood, R. L. Pigfood, C. R. Wilke, Mass Trasnfer, McGraw Hill, Inc., N.Y., 1975.
40. F. P. Incropera, D. P. De Witt, Fundamentals of Heat and Mass Transfer, 3rd edn, John Willey & Sons, N.Y., 1995.
41. T. Z. Fahedy, Principles of Electrochemical Reactor Analysis, Elsevier, N.Y., 1985.
42. M. Z. Zaki, Y. A. El-Taweel, A. A. Zaatout, M. Z. El-Abd, G. H. Sedahmed, *J. Electrochem. Soc.,* **138**, 430 (1991).
43. S. Piovano, U. Bohm, *J. Applied Electrochem*., **17** (1), 217 (1987).
44. P. H. Calderbank, M. B. Moo-Young, *Chem. Eng. Sci.,* **16,** 39 (1961).
45. V. G. Levich, Physicochemical Hydrodynamics, Prentice Hall, Englewood Cliffs, N. Y., 1962.

МАСООБМЕННИ ХАРАКТЕРИСТИКИ НА НОВ ЕКСТРАКТОР ТЕЧНОСТ-ТЕЧНОСТ С ВЪРТЯЩИ СЕ ДИСКОВЕ

А. С. Шехата, А. Х. Елшазли*, А. А. Заатут, Г. Х. Седахмед

Катедра по инженерна химия, Факултет по инженерство, Александрийски университет, Александрия, Египет

Постъпила на 5 май, 2010 г.; преработена на 3 януари, 2011

(Резюме)

Масообменните характеристики на контактор с въртящи се мрежести дискове са изследвани чрез измерване на скоростта на масопренос на оцетна киселина от разтвор на толуол във вода. Изследваните променливи са геометрични параметри на дисковете като брой на отворите и диаметър на телта, скорост на въртене, физични свойства на разтвора, аксиална скорост на потока и ефект на броя на наредените в пакет мрежи, съставящи един диск. За контактор с единичен въртящ се мрежест диск скоростта на масопренос се определя чрез уравнението:

$$Sh_m = 132.63\, Sc^{0.33}\, \mathrm{Re}_S^{\,0.25}\, \mathrm{Re}_F^{0.3} \left(\frac{r_h}{d_w} \right)^{-1.38}$$

За въртящи се дискове, съставени от няколко мрежи, коефициентът на масопренос намалява с увеличаване на броя на мрежите в пакет, съставящи диска. Едно сравнение на поведението по отношение на масообмена на въртящ се мрежест диск и въртящ се контактор с плътен диск (КПД), показва, че при дадени условия, скоростта на масопренос при въртящ се мрежест диск е по-висока от тази на контактор с въртящ се плътен диск с фактор от 13.8 - 28.4, в зависимост от условията на работа. Измервания на консумацията на механична енергия показват по-висок коефициент на масопренос, при по-висока консумация на енергия. Отбелязани са практически приложения на предложения екстрактор в области като фармацевтичната промишленост, хидрометалургия, петролната индустрия и обработка на вода.